JTTEE5 16:736–743
DOI: 10.1007/s11666-007-9101-0
1059-9630/$19.00 © ASM International

Peer Reviewed

3D Modeling of Transport Phenomena and the Injection of the Solution Droplets in the Solution Precursor Plasma Spraying

Yanguang Shan, Thomas W. Coyle, and Javad Mostaghimi

(Submitted March 11, 2007; in revised form June 18, 2007)

Solution precursor plasma spraying has been used to produce finely structured ceramic coatings with nano- and sub-micrometric features. This process involves the injection of a solution spray of ceramic salts into a DC plasma jet under atmospheric condition. During the process, the solvent vaporizes as the droplet travel downstream. Solid particles are finally formed due to the precipitation of the solute, and the particle are heated up and accelerated to the substrate to generate the coating. This article describes a 3D model to simulate the transport phenomena and the trajectory and heating of the solution spray in the process. The jet-spray two-way interactions are considered. A simplified model is employed to simulate the evolution process and the formation of the solid particle from the solution droplet in the plasma jet. The temperature and velocity fields of the jet are obtained and validated. The particle size, velocity, temperature, and position distribution on the substrate are predicted.

Keywords numerical simulation, solution precursor plasma spraying, two-way interactions, spray parameters

1. Introduction

Thermal plasma spraying technologies are used to produce various thick coatings. In conventional plasma spray process, a powder of the coating material to be formed is introduced into the plasma jet, in which micro-sized powder particles are melted and accelerated to the substrate to form the coating by stacking of individual lamellae. Recently, a new plasma spray coating method, solution precursor plasma spraying (SPPS), was used to generate finely structured ceramic coatings (Ref 1, 2). In this process, a solution spray of ceramic salts instead of ceramic powders is injected into the plasma jet either by atomization or by a liquid stream. Rapid heat up and evaporation of the solution droplets result in the formation of the solid particles, which are heated up and accelerated to the substrate to generate the coating. The properties of the coating highly depend on the process parameters, such as the torch operating conditions and injection parameters of the solution spray (Ref 3). In order to gain a better understanding of this process, a 3D model is developed to study the transport phenomena and the behavior of the solution spray in the process. The model was solved using Fluent CFD code (Ref 4). The temperature and velocity fields of the jet are obtained and validated. The particle size, velocity, temperature and position distribution on the substrate are predicted.

This article is an invited paper selected from presentations at the 2007 International Thermal Spray Conference and has been expanded from the original presentation. It is simultaneously published in *Global Coating Solutions, Proceedings of the 2007 International Thermal Spray Conference*, Beijing, China, May 14-16, 2007, Basil R. Marple, Margaret M. Hyland, Yuk-Chiu Lau, Chang-Jiu Li, Rogerio S. Lima, and Ghislain Montavon, Ed., ASM International, Materials Park, OH, 2007.

Yanguang Shan, School of Power Engineering, University of Shanghai for Science and Technology, Shanghai, China; and **Thomas W. Coyle** and **Javad Mostaghimi**, Centre for Advanced Coating Technologies, University of Toronto, Toronto, ON, Canada. Contact e-mail: y.shan@utoronto.ca.

2. Mathematical Models

2.1 Plasma Jet

The following assumptions are made in this model: (1) the flow is time-dependent, incompressible, and turbulent with temperature-dependent properties; (2) the plasma is in local thermodynamic equilibrium and optically thin; (3) two-way coupling between the plasma jet and the solution spray is considered; (4) the solution is introduced radially into the jet via a pressure atomizer, and no carrier gas is introduced.

The time-dependent equations to be solved for the gas phase are conservation of mass, momentum, energy, species, and turbulent kinetic energy as well as its dissipation as follows:

$$\frac{\mathrm{D}\rho}{\mathrm{D}t} + \rho\nabla\cdot\vec{u} = S_{\mathrm{C}}^{\mathrm{s}} \quad \text{(Eq 1)}$$

$$\rho\frac{\mathrm{D}\vec{u}}{\mathrm{D}t} = -\nabla P + \nabla\cdot\Gamma_{\mu}\nabla\vec{u} + \vec{S}_{\mathrm{M}}^{\mathrm{s}} \quad \text{(Eq 2)}$$

$$\rho\frac{\mathrm{D}h}{\mathrm{D}t} = \nabla\cdot\Gamma_{h}\nabla h - Q_{\mathrm{R}} + S_{\mathrm{E}}^{\mathrm{s}} \quad \text{(Eq 3)}$$

$$\rho\frac{DY}{Dt} = \nabla\cdot\Gamma_D\nabla Y + S_C^s \quad \text{(Eq 4)}$$

All the physical quantities in the foregoing equations are their time-averaged values. ρ is the gas density, t the time, P the pressure, h the enthalpy, $\vec{u}$ the velocity vector, Y the mass fraction, Q_R the radiation loss, and S_C^s,$\vec{S}_M^s$, and S_E^s, are the contributions of the solution spray to the equation of mass, momentum and energy, respectively. The conventional RNG-based k–ε model (Ref 4) is used to take into account the turbulent characteristics of the plasma jet. It is derived from the instantaneous Navier-Stokes equations using a mathematical technique called renormalization group (RNG) methods. The equations of turbulent kinetic energy and its dissipation are as follows:

$$\frac{\partial}{\partial t}(\rho k)+\frac{\partial}{\partial x_i}(\rho k u_i)=\frac{\partial}{\partial x_j}\left(\alpha_k\mu_{eff}\frac{\partial k}{\partial x_j}\right)+G_k+G_b-\rho\varepsilon - Y_M+S_k \quad \text{(Eq 5)}$$

$$\frac{\partial}{\partial t}(\rho\varepsilon)+\frac{\partial}{\partial x_i}(\rho\varepsilon u_i)=\frac{\partial}{\partial x_j}\left(\alpha_\varepsilon\mu_{eff}\frac{\partial \varepsilon}{\partial x_j}\right)+C_{1\varepsilon}\frac{\varepsilon}{k}(G_k+C_{3\varepsilon}G_b) - C_{2\varepsilon}^*\rho\frac{\varepsilon^2}{k}+S_\varepsilon \quad \text{(Eq 6)}$$

where $C_{2\varepsilon}^* = C_{2\varepsilon}+(C_\mu\eta^3(1-\eta/\eta_0)/1+\beta\eta^3)$, $\eta = S\cdot k/\varepsilon$, $S=\sqrt{2S_{ij}S_{ij}}$, $S_{ij}=12(u_{i,j}+u_{j,i})$, $\eta_0=4.38$, $\beta=0.012$. The inverse effective Prandtl numbers α_k and α_ε are set equal to 1.393. The effective viscosity is given by $\mu_{eff}=\mu+\mu_t$, in which $\mu_t=\rho C_\mu k^2/\varepsilon$ and $C_\mu=0.0845$. $C_{1\varepsilon}$ and $C_{2\varepsilon}$ are set as 1.42 and 1.68, respectively. All of these values are derived analytically from RNG theory. G_k represents the generation of turbulent kinetic energy due to the mean velocity gradient, G_b is the generation of turbulence due to buoyancy. Y_M represents the effect of compressibility on turbulence, which is neglected in this work. S_k and S_ε are source terms. $C_{3\varepsilon}$ is not specified, but is rather calculated (Ref 4). For more comprehensive description of RNG theory and its application to turbulence, please refer to Ref 5.

The temperature-dependent transport and thermodynamic properties of Ar and Air at atmospheric pressure are obtained from Ref 6. The mixing rule is used to take into account the effect of the mixing of solvent vapor on the properties of the plasma jet.

2.2 Computational Domain, Initial and Boundary Conditions

The computational domain and grid used in the calculation is shown in Fig. 1. To capture the large gradient near the torch exit and on the central axis, non-uniform mesh is used. The computational domain is 20 mm × 2 π × 150 mm according to the ($r\times\theta\times z$) cylindrical coordinate system.

The temperature and velocity profiles at the exit of the torch are assumed as following (Ref 7)

$$v=0,\quad w=0,\quad \text{and}\quad u=u_m\left(1-\left(\frac{r}{R}\right)^m\right) \quad \text{(Eq 7)}$$

$$T=(T_m-T_w)\left(1-\left(\frac{r}{R}\right)^n\right)+T_w \quad \text{(Eq 8)}$$

where T_m and u_m are maximum temperature and velocity at the centerline of the gun exit, respectively. No swirl component is considered. m and n are the power-law exponents, which are determined from global mass and total enthalpy conservation. In this method, m and n are first assumed, then Eq 7 and 8 are used to calculate the radial distributions of the velocity and temperature at the exit of the plasma gun. If the calculated gas flow rate and enthalpy of the plasma equal to the measured gas flow rate and enthalpy of the plasma, the values of m and n are obtained. The details of this method can be found in Ref 7. R is the nozzle radius, T_w is the torch wall temperature. A uniform turbulent intensity (2%) and torch diameter are given to specify the turbulence conditions at the torch exit. For the solid wall, $u=v=w=0$, $T=T_w$. For the side boundary and outlet boundary, the pressure inlet and pressure outlet boundary conditions are applied, respectively. In the case of an impinging jet, the wall boundary condition in Fluent code is employed on the substrate. Before the calculation, a solution from a steady state case is set as initial condition.

2.3 Solution Droplet Evolution

The injection of particles or droplets into the plasma is an important application of plasma technology. A lot of articles (e.g., Ref 8-20) have been published on the trajectory and heating of particles or droplets in thermal plasma spraying processes. Different expressions of particle drag force and heat transfer were proposed by different authors. Those expressions differ in whether or not they take into account the plasma-particle interactions, the turbulent dispersion, the internal heat conduction, the thermophoretic force, and the rarefaction effect. Little numerical work was done on the injection of solution droplets into the plasma. To simulate the trajectories and the heat and mass transfer of the solution droplet, the following assumptions are employed in this work: (1) the solution droplet is spherical symmetric and the gas film around the solution droplet has uniform physical properties; (2) the temperature within the solution droplet and the pressure around the solution droplet are assumed to be uniform; (3) the solution droplet surface is under thermal equilibrium state; (4) the radiation effect is neglected on the heating of the solution droplet; (5) the rarefaction effect is neglected; and (6) the evaporation of the solute is neglected.

Lagrangian equations of motion and heat and mass transfer are used to simulate the solution droplet behavior in the plasma jet. Interactions between the spray and the jet are considered by adding proper exchange terms in the governing equations of the plasma jet. Droplet breakup and collision during the spray evolution are neglected. The dispersion of the droplets due to turbulence is included using the stochastic tracking approach.

2.3.1 Droplet Motion. The velocity of a droplet can be calculated from the force balance on the droplet.

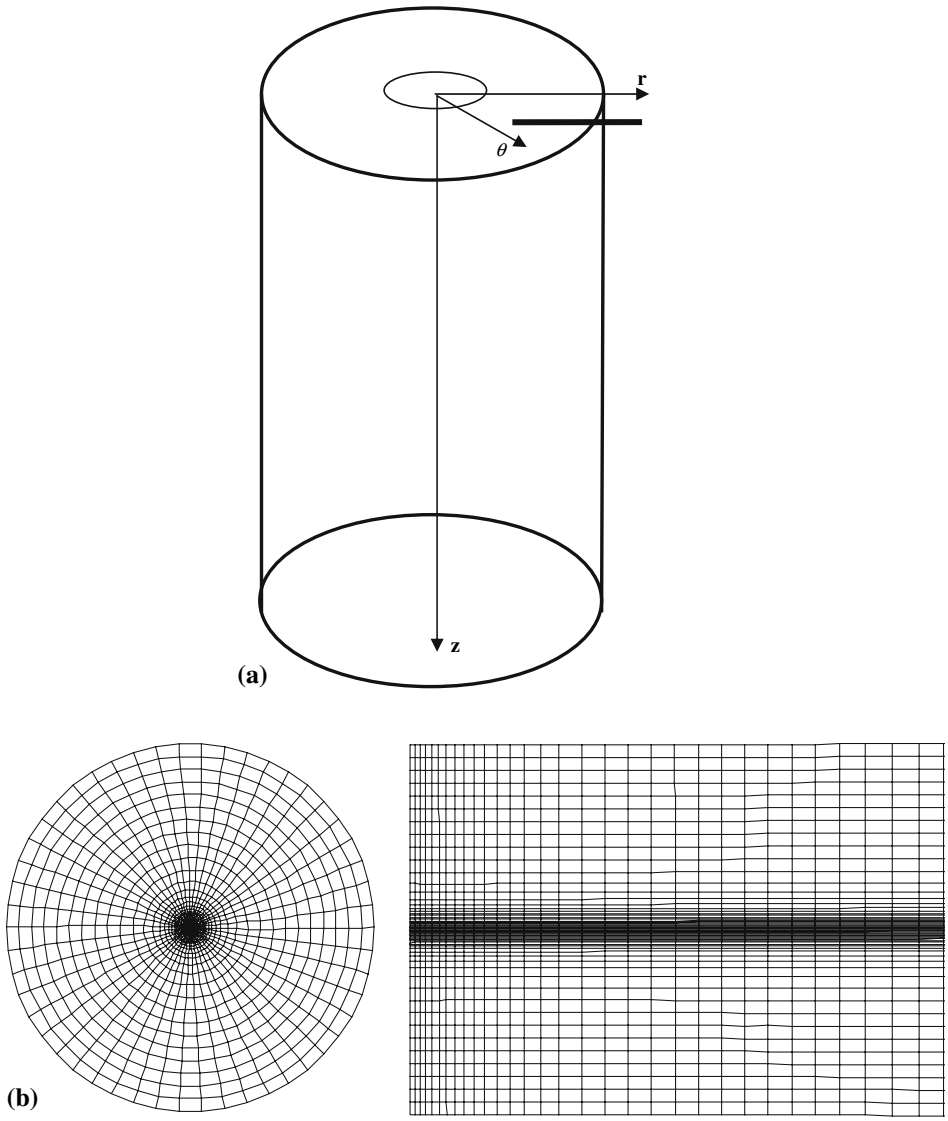

Fig. 1 3D computational domain (a) and computational mesh (b)

$$\frac{du_d}{dt} = F_D(u - u_d) + \frac{g_x(\rho_d - \rho)}{\rho_d} + F_x \qquad \text{(Eq 9)}$$

where $F_D(u - u_d)$ is the drag force per unit droplet mass, and $F_D = (18\mu/\rho_d d_d^2)(C_D Re/24)$ $(0.1 \le Re \le 5.0 \times 10^4)$. The relative Reynolds number Re is defined as $Re = (\rho|u_d - u|d_d/\mu)$. F_x is an additional acceleration term. u, μ and ρ are fluid velocity, viscosity and density, respectively. u_d and ρ_d are droplet velocity and density, respectively. Since the thermophoretic force is usually small comparing with the aerodynamic drag force (Ref 8), only the aerodynamic drag force and gravitational force are considered in this work. The drag coefficient is calculated by the correlation of Morsi and Alexander (Ref 21).

2.3.2 Droplet Heat and Mass Transfer. When the solution droplet penetrates into the plasma jet, it is heated up rapidly. Evaporation takes place from the surface of the droplet. As a result, the droplet loses the solvent, and higher concentration solute builds up on the droplet surface. When the droplet temperature reaches its boiling point, the boiling process begins and the solvent goes away from the droplet more quickly. With increasing solute concentration in the droplet, saturation and supersaturation levels of the solute concentrations are reached, and finally the solution droplet forms a solid particle when all the solvent goes away. An individual solution droplet experiences the following heating processes when it is injected into the plasma jet: (1) inert heating, (2) vaporization, (3) boiling, (4) solid particle forms, and (5) particle heating (melting). During the inert heating stage, no mass transfer occurs. The droplet temperature is lower than the vaporization temperature. It is calculated by heat balance equation neglecting radiation effect as follows:

$$m_d c_d \frac{dT_d}{dt} = hA_d(T_f - T_d) \quad \text{(Eq 10)}$$

where m_d is the mass, A_d the surface area, c_d the heat capacity, and T_d is the temperature of the solution droplet, respectively. T_f is the temperature of the plasma gas. h is convective heat transfer coefficient. After the droplet temperature reaches its vaporization temperature, the rate of vaporization is governed by gradient diffusion, which is given by

$$\frac{dm_d}{dt} = -k_c A_d M_d (C_s - C_\infty) \quad \text{(Eq 11)}$$

where k_c is the mass transfer coefficient, M_d the molecular weight of the solvent, and C_s and C_∞ are vapor concentration of the solvent at the solution droplet surface and in the plasma jet, respectively. The droplet temperature is determined by:

$$m_d c_d \frac{dT_d}{dt} = hA_d(T_f - T_d) + \frac{dm_d}{dt} h_{fg} \quad \text{(Eq 12)}$$

where h_{fg} is latent heat. When the temperature of the droplet reaches the boiling point, the droplet remains at its boiling temperature. A boiling rate equation is applied to calculate the mass transfer as follows (Ref 22).

$$\frac{d(d_d)}{dt} = \frac{4k_f(1 + 0.23\sqrt{Re_d})}{\rho_d c_f d_d} \ln\left[1 + \frac{c_f(T_f - T_d)}{h_{fg}}\right] \quad \text{(Eq 13)}$$

where d_d is the droplet diameter, k_f is thermal conductivity of the plasma gas, and c_f is the heat capacity of the plasma gas.

When all the solvent goes away, the model assumes that the solution droplet forms a solid particle, and the precipitation and nucleation process is ignored. At this point, the model set all the properties of the droplet as that of the solid particle. The mass (diameter) of the particle is calculated according to the mass fraction or volume fraction of the solute in the solution. Then, the heating of the particle can be calculated by Eq 10. When the particle reaches its melting point, its temperature is set to the melting point, and no mass transfer is calculated.

2.3.3 Initial and Boundary Conditions. At the solution injector exit, droplet size distribution is determined based on the experiment observation. The initial temperature, mass flow rate of the solution spray, and injection velocity are specified at the injector exit. During the calculation, if a droplet hits a wall, the ''TRAP'' boundary condition applies, which terminates the trajectory calculations and records the droplet as ''trapped''. To simplify the calculation, the entire mass of the droplet is assumed to instantaneously pass into the vapor phase and enter the cell adjacent to the boundary. If a droplet crosses a free boundary or flow boundary, the ''ESCAPE'' boundary condition applies, which reports the droplet as having ''escaped'' when it encounters the boundary. Trajectory calculations are terminated.

3. Numerical Technique

Fluent V6.2 code (Ref 4) is used to solve the governing equations of the plasma jet using control volume method. The second order upwind scheme is used for the convective terms. The SIMPLE algorithm of Patankar (Ref 23) is chose for the pressure-velocity coupling. The method used for solving the spray evolution is based on the ideas of Monte Carlo method and of discrete parcel method (Ref 15). The droplet parcels are introduced into the plasma jet during the time of injection. Each parcel is composed of a number of droplets with same properties. The parcels are sampled randomly from assumed probability distributions that govern droplet properties at injection and droplet behavior after injection. An adequate statistical representation of realistic sprays can be obtained when a sufficiently large number of computational parcels are used. To consider the effect of the heat, mass, and momentum exchange between the spray and the plasma jet, Two-way coupling is accomplished by alternately solving the discrete and continuous phase equations until the solutions in both phases have stopped changing.

4. Results and Discussion

4.1 Validity of the Plasma Jet Model

To show the validity of the plasma jet model, the predictions of this model were compared with the experimental results (Ref 7). In the experiment, a SG-100 spraying gun was operated at 19.6 kW ($U = 28$ V, $I = 700$A) with argon flow rate of $m = 0.001$ kg/s. The thermal efficiency of the spraying gun is around 40%. The argon plasma jet discharges into air environment. The obtained values of centerline velocity and temperature are 1090 m/s and 13,490 K, respectively. m and n in Eq 7 and 8 are set to 2.6 and 7.8, respectively (Ref 7). The diameter of the torch exit is 7.8 mm. This domain is divided into $22 \times 50 \times 40$ grids points according to the $(r \times \theta \times z)$

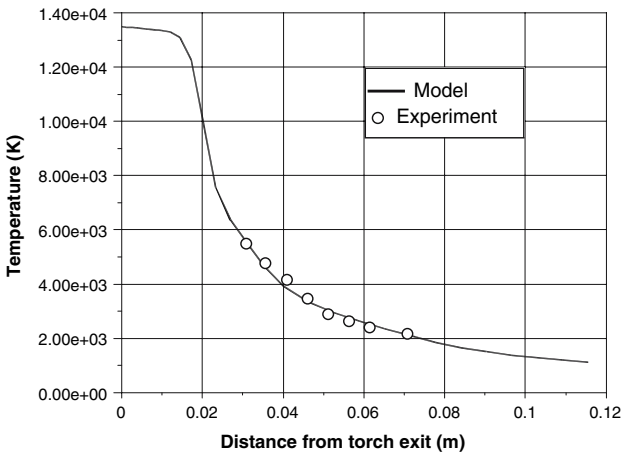

Fig. 2 Centerline temperature of the jet

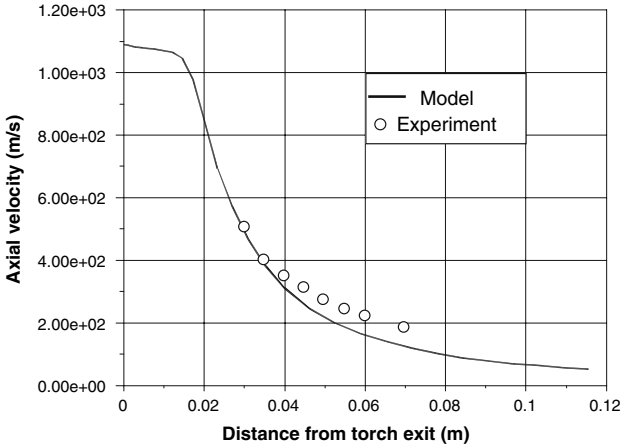

Fig. 3 Centerline velocity of the jet

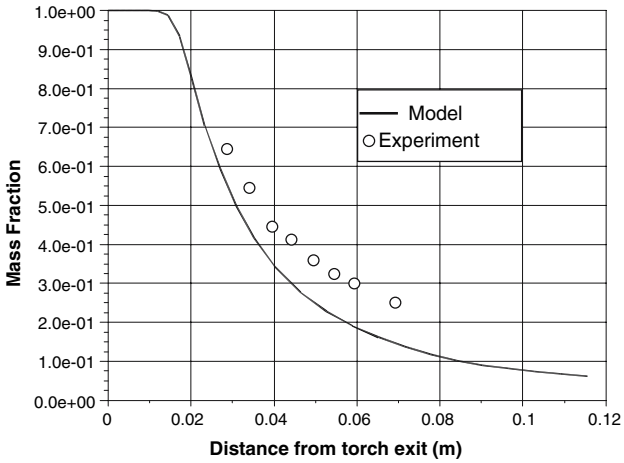

Fig. 4 Centerline Ar mass fraction of the jet

cylindrical coordinate system. Fig. 2-4 show the comparisons of the centerline axial velocity (Fig. 2), temperature (Fig. 3), and argon mass fraction (Fig. 4) between the model results and the experiment. It can be seen that the agreement between the model results and experimental measurements is relatively good downstream of the jet core. The discrepancies come from the uncertainty and the measurement error of the experiment and the model assumptions, which are described elsewhere (Ref 7, 24).

4.2 Effect of the Injection of the Spray on the Jet

In following sections, a solution spray is injected into the plasma jet. The spray gun is operated at $U = 48$ V, $I = 550$ A, with Ar flow rate of 62 slpm and H_2 flow rate of 2 slpm. The mass flow rate of the plasma gas is 0.0018 kg/s. $U_m = 1000$ m/s, $T_m = 11{,}500$ K. m and n in Eq 7 and 8 are set to 2. The jet impinges onto a substrate locates 60 mm away from the torch exit. The injector locates at position (0.01 m, 0°, 0.005 m) as shown in Fig. 1. The solution mass flow rate is 0.0002 kg/s. The concentration of the solution is 0.5 M. The solvent is water. The final product of the solute

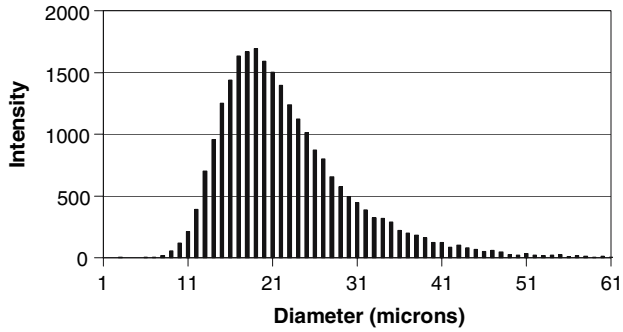

Fig. 5 Droplet size distribution of the solution spray

is $(La_{0.85}Sr_{0.15})MnO_3$ (LSM) (specific mass: 6570 kg/m^3, specific heat 573 J/kg K, thermal conductivity 4 W/m K, melting temperature 2153 K (Ref 25)). Initial droplet size distribution is chose based on the experiment observation, which is shown in Fig 5. The minimum droplet diameter is set to 5 μm and the maximum droplet diameter is set to 60 μm. The injection velocity is 20-50 m/s. The initial solution temperature is 300 K.

To show the effect of the injection of the solution spray on the plasma jet, the local deformations of temperature and axial velocity are shown in Fig 6(a) and (b), respectively. The deformation near the injector is evident. This is due to the exchange of energy, momentum, and mass between the spray and the plasma jet. Usually, the bigger droplet penetrates into the jet further than the small one at the same injection velocity, and a small injection cone results in stronger local deformation of the flow and temperature fields.

4.3 Droplet/Particle Conditions on the Substrate

The same case as previously is simulated in this section. The droplet/particle size, velocity, temperature and position distribution at the spray distance are predicted in this section.

4.3.1 Droplet/Particle Size Distribution on the Substrate. Figure 7 shows the computed droplet/particle size distribution on the cross-section at $z = 60$ mm. The results indicate that most of the droplet/particle sizes are below 10 μm at this position, while some droplets/particles with diameter larger than 25 μm are present on the substrate. The reason is that bigger droplets have higher momentum than the small ones at the same injection velocities at the injector exit, these droplet may go through the hot core volume of the jet. As a result, these droplets are not heated by the jet effectively. Besides, under real conditions, such large droplets should break up due to shear stresses, but in this model, this mechanism is not taken into consideration. Therefore, the results are rough indications, and droplet breakup should be taken into account in further study.

4.3.2 Droplet/Particle Temperature Distribution on the Substrate. Figure 8 shows the computed droplet/particle temperature distribution on the cross-section at $z = 60$ mm. As we can see, the temperature of a large

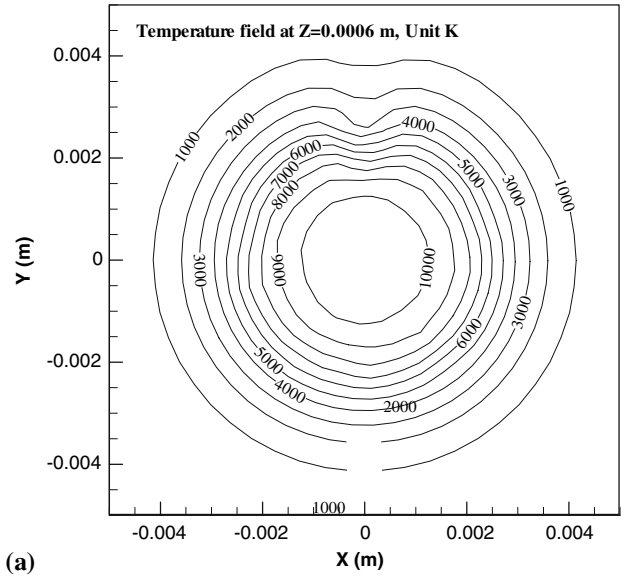

(a)

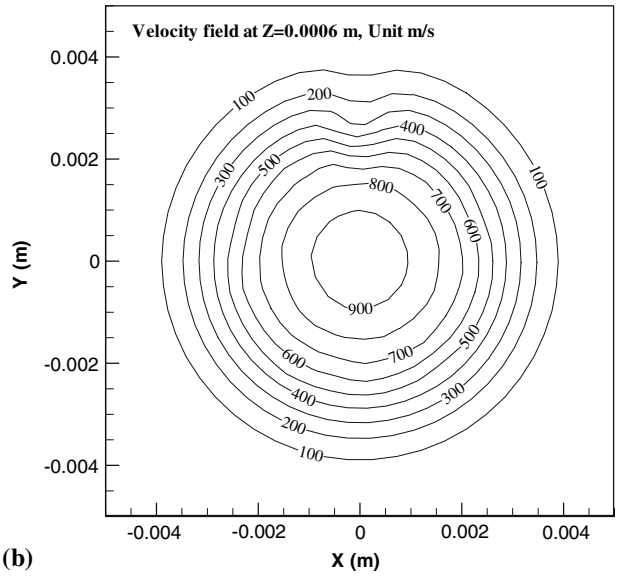

(b)

Fig. 6 Computed deformation of temperature (a) and axial velocity field (b) due to the spray injection

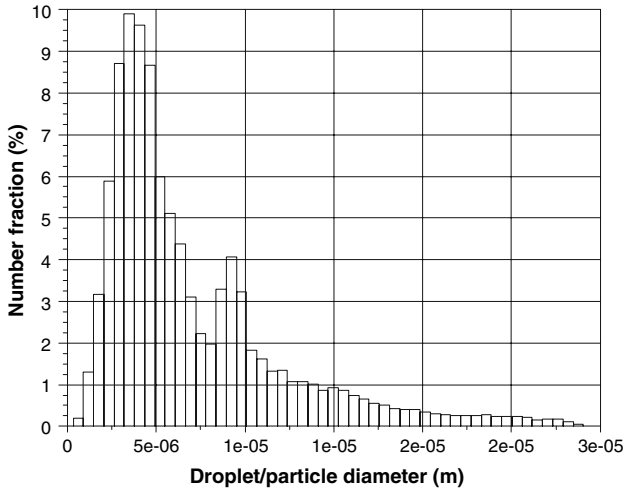

Fig. 7 Computed droplet/particle size distribution on the substrate ($z = 60$ mm)

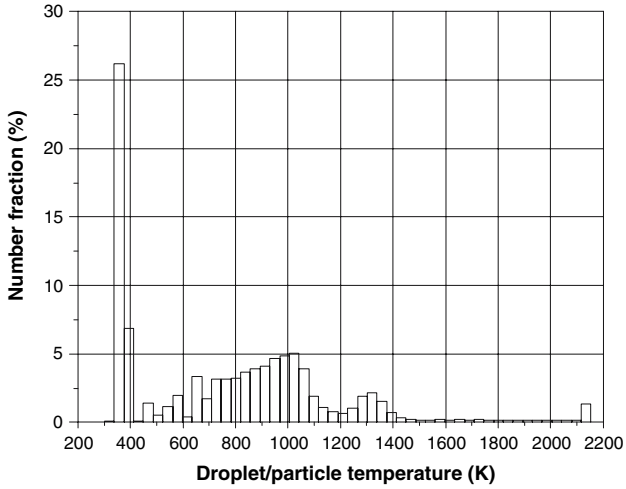

Fig. 8 Computed droplet/particle temperature distribution on the substrate ($z = 60$ mm)

portion of droplets (~25%) is less than 400 K. This indicates these droplets should arrive on the substrate in a state of liquid solution, and their temperatures remain at the boiling point of the solvent. These droplets are further exposed to the hot plasma jet as the jet scans the substrate during the spray. Decomposition of these droplets results in the micro- and nano-size voids that constitute the porosity in the coating micro-structure (Ref 20, 26). It also can be seen from Fig. 8 that just a small portion of the particle reaches their melting point. The temperatures of most of the particle are between 600 and 1400 K. This indicates that under the condition used in this work, the deposition efficiency could be fairly low since the particles are not fully melted. The relative low particles temperature also can be explained by calculating the residence time of the droplets/particles in the jet, which is shown in Fig. 9. It can be seen that the residence time of most of the droplets/particles are less than 1 ms, which is small. This result also indicates the injection conditions are not good. Therefore, to increase the deposition efficiency, it is necessary to optimizing the injection parameters and the operating conditions of the plasma gun to heat up droplets/particles effectively in the jet.

4.3.3 Droplet/Particle Axial Velocity Distribution on the Substrate. Figure 10 shows the computed droplet/particle axial velocity distribution on the cross-section at $z = 60$ mm. It can be seen that the velocities of most of the droplets/particles are between 50 and 350 m/s. The bigger droplets and the droplets close to the center axis gain high momentum from the jet, these droplets remain a higher velocity. The smaller droplets and the droplet at the fringe of the jet gain low momentum from the jet, these droplets remain a lower velocity. The velocity gradient of the jet on the plane perpendicular to the jet becomes small when the

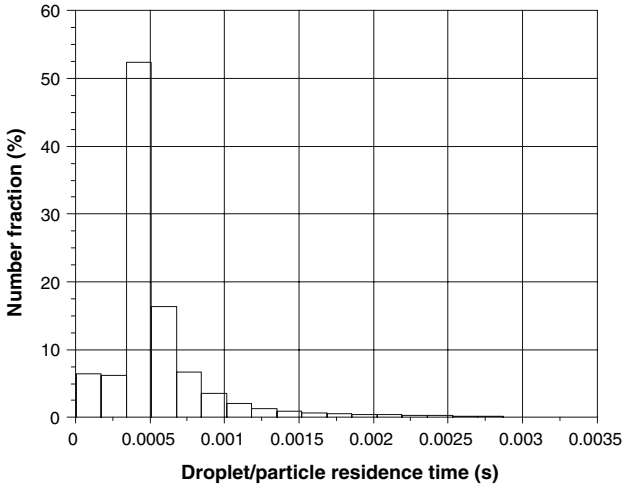

Fig. 9 Computed droplet/particle residence time in the jet

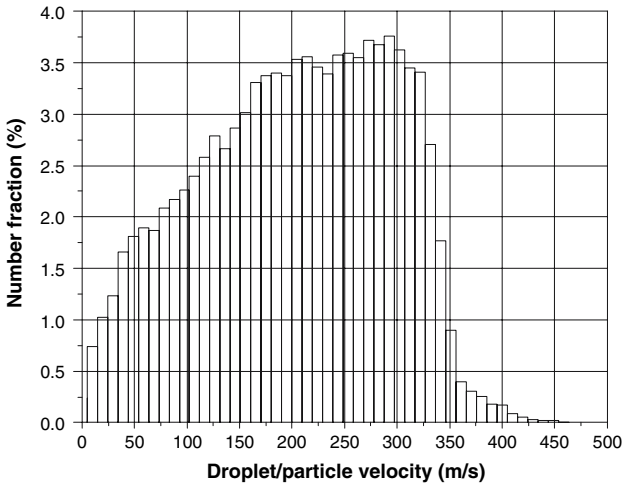

Fig. 10 Computed droplet/particle axial velocity distribution on the substrate ($z = 60$ mm)

jet is fully developed. As a result, the distribution of the velocity will become uniform downstream of the jet.

4.3.4 Droplet/Particle Position Distribution on the Substrate. Figure 11 shows the computed droplet/particle X-coordinate (Fig. 11(a)) and Y-coordinate (Fig. 11(b)) position distribution on the cross-section at $z = 60$ mm. It can be seen the droplet/particle distribution on X-coordinate is almost symmetric by the centerline, while the droplet/particle distribution on Y-coordinate has an offset from the centerline. Since the injector locates at the position (0.01 m, 0°, 0.005 m), it is understandable to observe the offset.

5. Conclusions

A 3D model has been developed to study the transport phenomena and the trajectory and heating of solution droplets in SPPS. The predicted temperature, velocity,

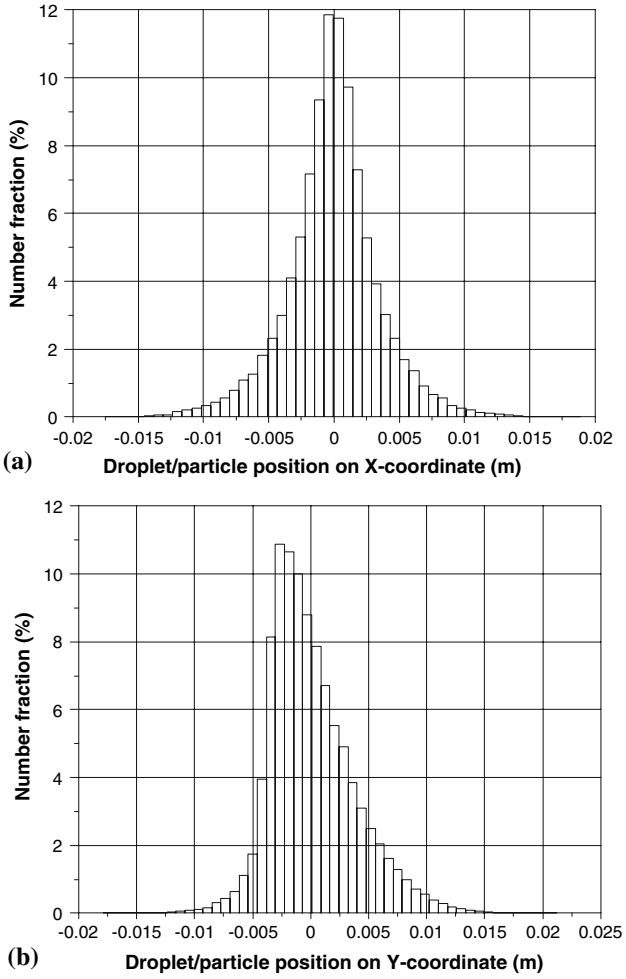

Fig. 11 Computed droplet/particle position distribution on the substrate ($z = 60$ mm)

and Ar mass fraction on the centerline of the plasma jet are compared with experiments. The agreement is fairly good. The injection of a solution spray into the plasma jet is also studied. The results show evident effects of the injection of the spray on the plasma jet flow and temperature field. The droplet/particle size, velocity, temperature and position distributions on the substrate are predicted. The results show some droplets should arrive on the substrate in a state of liquid. These droplets may result in the micro- and nano-sized voids that constitute the porosity usually observed in the coating micro-structure. It is also shown that just a small portion of the particle reaches their melting point. The temperatures of most of the particle are less than the melting point under the conditions used in this work.

Acknowledgments

The financial support of the NSERC of Canada, the National Natural Science Foundation of China (Project 50706027), and the Shanghai Municipal Education Commission (Project 05EZ16) is gratefully acknowledged.

References

1. J. Karthikeyan, C.C. Berndt, S. Reddy, J.Y. Wang, A.H. King, and H. Herman, Nano-material Deposits Formed by DC Plasma Spraying of Liquid Feedstocks, *J. Am. Ceram. Soc.*, 1998, **81**, p 121-128
2. N. Padture, K. Schlichting, T. Bhatia, A. Ozturk, B. Cetegen, E. Jordan, and M. Gell, Towards Durable Thermal Barrier Coatings with Novel Microstructures Deposited by Solution Precursor Plasma Spray, *Acta Mater.*, 2001, **49**, p 2251-2257
3. L. Xie, X. Ma, A. Ozturk, E. Jordan, N. Padture, B. Cetegen, D. Xiao, and M. Gell, Processing Parameter Effects on Solution Precursor Plasma Spray Process Spray Patterns, *Surf. Coat. Technol.*, 2004, **183**, p 51-61
4. Fluent Inc., *Fluent V6.2 User's Guide* (Lebanon, NH, USA), 2005
5. D. Choudhury, *Introduction to the Renormalization Group Method and Turbulence Modeling*, Fluent Inc. Technical Memorandum TM-107 (Lebanon, NH, USA), 1993
6. M.I. Boulos, P. Fauchais, and E. Pfender, Thermal Plasmas: Fundamentals and Applications, Vol 1. Plenum, New York, 1994
7. M. Jankovic, Study of Atmospheric Plasma Spray Process with the Emphasis on Gas Shrouded Nozzles, PhD Thesis, University of Toronto, 1996
8. E. Pfender and Y.C. Lee, Particle Dynamics and Particle Heat and Mass Transfer in Thermal Plasmas. Part I. The Motion of a Single Particle without Thermal Effects, *Plasma Chem. Plasma Process.*, 1985, **5**, p 211-237
9. Y.C. Lee, Y.P. Chyou, and E. Pfender, Particle Dynamics and Particle Heat and Mass Transfer in Thermal Plasmas. Part II. Particle Heat and Mass Transfer in Thermal Plasmas, *Plasma Chem. Plasma Process.*, 1985, **5**, p 391-416
10. X. Chen and E. Pfender, Behavior of Small Particles in a Thermal Plasma Flow, *Plasma Chem. Plasma Process.*, 1983, **3**, p 351-366
11. P. Proulx, J. Mostaghimi, and M.I. Boulos, Heating of Powders in an RF Inductively Coupled Plasma under Dense Loading Conditions , *Plasma Chem. Plasma Process.*, 1987, **7**, p 29-52
12. R. Ye, P. Proulx, and M.I. Boulos, Particle Turbulent Dispersion and Loading Effects in an Inductively Coupled Radio Frequency Plasma, *J. Phys. D: Appl. Phys.*, 2000, **33**, p 2154-2162
13. A. Vardelle, P. Fauchais, B. Dussoubs, and N. Themelis, Heat Generation and Particle Injection in a Thermal Plasma Torch, *Plasma Chem. Plasma Process.*, 1998, **18**, p 551-574
14. J. Fazilleau, C. Delbos, V. Rat, J.F. Coudert, P. Fauchais, and B. Pateyron, Phenomena Involved in Suspension Plasma Spraying, *Plasma Chem. Plasma Process.*, 2006, **26**, p 371-391
15. Y. Shan and J. Mostaghimi, Numerical Simulation of Aerosol Droplets Desolvation in a Radio Frequency Inductively Coupled Plasma, *Spectrochim. Acta, Part B*, 2003, **58**, p 1959-1977
16. Y. Shan and J. Mostaghimi, Modeling Dense Liquid Sprays in Radio Frequency Inductively Coupled Plasmas, *Plasma Chem. Plasma Process.*, 2005, **25**, p 193-214
17. H.-P. Li and X. Chen, Three-dimensional Modeling of the Turbulent Plasma Jet Impinging upon a Flat Plate and with Transverse Particle and Carrier-gas Injection, *Plasma Chem. Plasma Process.*, 2002, **22**, p 27-58
18. K. Ramachandran, T. Sato, and H. Nishiyama, 3D Modeling of Evaporation of Water Injected into a Plasma Jet, *Int. J. Heat Mass Transfer*, 2003, **46**, p 1653-1663
19. K. Ramachandran, N. Kikukawa, and H. Nishiyama, 3D Modeling of Plasma–particle Interactions in a Plasma Jet under Dense Loading Conditions, *Thin Solid Films*, 2003, **435**, p 298-306
20. A. Ozturk and B.M. Cetegen, Modeling of Axially and Transversely Injected Precursor Droplets into a Plasma Environment, *International Journal of Heat and Mass Transfer*, 2005, **48**, p 4367-4383
21. S.A. Morsi and A.J. Alexander, An Investigation of Particle Trajectories in Two-phase Flow Systems, *J. Fluid Mech.*, 1972, **55**, p 193-208
22. K.K.Y. Kuo, Principles of Combustion. John Wiley and Sons, New York, 1986
23. S.V. Patankar, Numerical Fluid Flow and Heat Transfer. McGraw–Hill, New York, 1980
24. M. Jankovic and J. Mostaghimi, Thermally Induced Measurement Error by a Water-Cooled Enthalpy, *Plasma Chem. Plasma Proces.*, 1998, **18**, p 53-71
25. L. Petruzzi, S. Cocchi, and F. Fineschi, A Global Thermo-electrochemical Model for SOFC Systems Design and Engineering, *J. Power Sources*, 2003, **118**, p 96-107
26. L. Xie, E.H. Jordan, N.P. Padture, and M. Gell, Phase and Microstructural Stability of Solution Precursor Plasma Sprayed Thermal Barrier Coatings, *Mater. Sci. Eng. A*, 2004, **381**, p 189-195